Article

Investigating Seawater Intrusion in Republic of South Africa's Heuningnes, Cape Agulhas Using Hydrogeochemistry and Seawater Fraction Techniques

Abongile Xaza [1], Harold Wilson Tumwitike Mapoma [2], Tamiru A. Abiye [3], Sumaya Clarke [1] and Thokozani Kanyerere [1,*]

1   Department of Earth Sciences, University of the Western Cape, Bellville 7535, South Africa; 3469797@myuwc.ac.za (A.X.); sclarke@uwc.ac.za (S.C.)
2   Department of Physics and Biochemical Sciences, Malawi University of Business and Applied Sciences, Private Bag 303, Blantyre 312225, Malawi; hmapoma@mubas.ac.mw
3   School of Geosciences, University of the Witwatersrand, Johannesburg 2050, South Africa; tamiru.abiye@wits.ac.za
*   Correspondence: tkanyerere@uwc.ac.za

Abstract: The Heuningnes Catchment in the Republic of South Africa was used as a case study in this research to describe the application of saltwater fraction/quantification and hydrogeochemistry methods to evaluate the extent of saline intrusion in the coastal aquifers. The argument of the research is that the presence of seawater incursion may be conclusively determined by combining the examination of the major ions, seawater fraction, stable isotopes of water, bromide, and geochemical modeling. Using stable isotopes of oxygen (^{18}O) and deuterium (^{2}H), major ions chemistry, seawater composition, and geochemical modeling, the genesis of salinity and mixing of different water masses were examined. Twenty-nine (29) samples of groundwater were examined. All samples showed water facies of the Na-Cl type, indicating a seawater-related origin. The significance of mixing in coastal aquifers under natural conditions was shown by the hydrogeochemical characteristics of key ions derived from ionic ratios, which demonstrated substantial adherence to mixing lines among endmembers for freshwater as well as saltwater (seawater). The quantification of seawater contribution in groundwater percentages varied from 0.01 to 43%, with three samples having concentrations of seawater above 50%. It was clear from the hydrogeochemical analysis and determination of the proportion of saltwater that the seawater intrusion impacted the coastal fresh groundwater. In addition, the chloride concentration in the groundwater ranged from 81.5 to 26,557.5 mg/L, with the corresponding δ^{18}O values ranging from -5.5‰ to -0.9‰, which suggested that freshwater and saltwater were mixing. The Br^{-}/Cl^{-} ratios showed that evaporation had played a part in elevating groundwater salinity as well. Since saturation indices were below zero, the mineral dissolution could also contribute to the salinization of groundwater. Further proof of seawater incursion in the investigated catchment was supplied by geochemical modeling and bromide. Even though such tools were not verified in multiple coastal aquifers for widespread generalization, the study offered a scientifically significant understanding of the application of such tools on seawater intrusion in coastal aquifers and has useful recommendations for the aquifer setting of similar environments.

Keywords: groundwater; hydrochemistry; isotopic analysis; PHREEQC; salinization; seawater quantification

1. Introduction

In coastal aquifers, seawater intrusion (SWI) is a prevalent concern everywhere in the world that can be caused by both static changes in the groundwater table and dynamically by incoming saline waters during pumping [1]). Throughout the past few decades, the salinity issue has received extensive research attention, especially in coastal aquifers [2].

Seawater intrusion into freshwater aquifers can cause water quality to deteriorate and put human infrastructure at risk of corrosion. One of the central problems with water quality in unconfined aquifers linked to the ocean is saltwater intrusion, specifically in cases when excess abstraction may result in a drop in the piezometric head. Owing to the presence of (i) clay layers, which at least partly separate groundwater from seawater, and (ii) a vadose zone, where most biogeochemical processes occur, hydrogeological activities in confined or semi-confined aquifers are more complex. Consequently, both confined and unconfined aquifers are susceptible to saltwater intrusion [3]. Aquifer water quality may also be affected by a series of exchange, dissolution, and precipitation reactions related to seawater intrusion [1]. Cation exchange processes are well recognized to occur in conjunction with the displacement of freshwater by saltwater during seawater intrusion [4].

The behavior of saline groundwater flow has been described in previous research using a mixture of chemical and isotopic markers, defining flow patterns, and identifying groundwater salinization processes [5–7]. Their application includes studying how the freshwater–saltwater interface moves and comprehending how various coastal aquifers' saline water bodies and surrounding freshwater interact with one another. Understanding the intricacy and non-linearity of saltwater intrusion in the coastal area is challenging due to the numerous elements that could be responsible for the salinity of groundwater. Examples include mineral weathering, saline groundwater moving to unconfined aquifers as a product of over-pumping, temperature changes and variations, and sea level rise. Another example is the evaporation of materials in wet places [8]. An increase in Cl^- and TDS concentrations along the shoreline can be a sign of seawater incursion. Seawater intrusion, which is the mixing of saline water and freshwater, and water–rock interactions can all have an impact on groundwater salinity (such as cation exchange processes with clays). The understanding of seawater intrusion mechanisms may be considerably improved by combining data from numerous sources with hydrogeological and chemical information. Research conducted elsewhere has mostly focused on groundwater flow modeling, brine water formation, and preventative strategies for seawater intrusion [9]. At the Heuningnes Catchment, however, there is limited knowledge of how much seawater is present. Seawater intrusion is now assessed using conventional hydrogeochemical techniques such as the single index, multivariate analysis, mathematical statistics, and attribute identification approaches. On the other hand, the single index method's calculation outputs have some drawbacks, including unpredictability and bias. This calls for new approaches to research the SWI process in the Heuningnes Catchment. Determining the saturation index (SI) in the Heuningnes Catchment using both the isotope technique and conventional hydrogeochemistry was the aim of this work as a result. It should be emphasized that this is the first time the Heuningnes Catchment's SI has been studied using the seawater quantification approach. In the research, geochemical modeling was also used.

2. Study Area

The Heuningnes catchment is situated in the Cape Agulhas Municipality, at 34°20″ and 34°50″ S latitude and 19°30″ and 20°30″ E longitude [10]. The catchment is 1401 km² in size and includes the quaternary catchments G50B, G50C, D, E, and F (Figure 1a). Due to the poor aquifer condition of the Bokkeveld Group shale, the little water that is extracted from it typically has brackish or saline quality. This formation can be found in the catchment's central region close to Elim village on the Agulhas Plain [11]. The Bokkeveld Group shale is covered by the Bredasdorp Group (Quaternary sediments) in the Heuningnes catchment, closer to the Soetandalsvlei Nature Reserve. The Bredasdorp deposits are composed of the tertiary and quaternary layers of unconsolidated to semi-consolidated, calcareous sands. The Bredasdorp Group's shallow marine and aeolian sediments also contribute to the primary aquifer in the catchment (Figure 1b).

There are primary and secondary aquifers within the catchment. Primary aquifers are created by unconsolidated sediments that have been deposited as alluvium in the

floodplains of important river systems [12]. These aquifers are frequently found in areas with low rainfall, and they are mostly refilled during strong rains and flooding.

Yet, secondary aquifers are the most prevalent and typical. They are composed of the Bokkeveld Group shale and Table Mountain Group (TMG) quartzites. These aquifers host groundwater in fractures (joints and fault networks) [13]. The TMG aquifers (quartzites) generally produce a substantial yield with good water quality, which has low TDS. On the other hand, the Bokkeveld aquifers (composed of shale) are characterized by low yield, poor water quality, and a high TDS [14]. In the Heuningnes Catchment, the most prominent aquifers are represented by the alluvial (primary) and fractured aquifers (secondary). The TMG is the Heuningnes Catchment's main source of groundwater (Table 1). There are other "small aquifers", but they do not provide significant water.
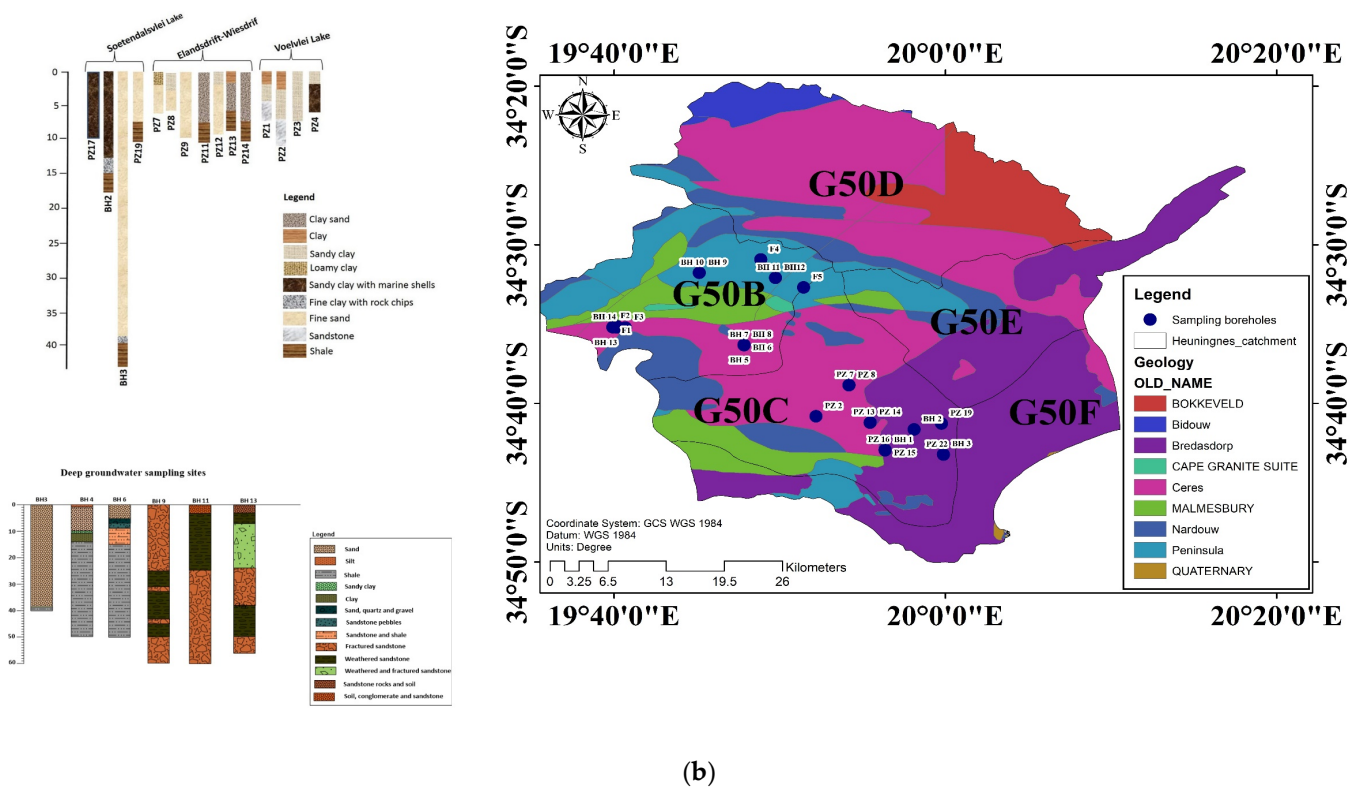

(**a**)

Figure 1. *Cont.*

(**b**)
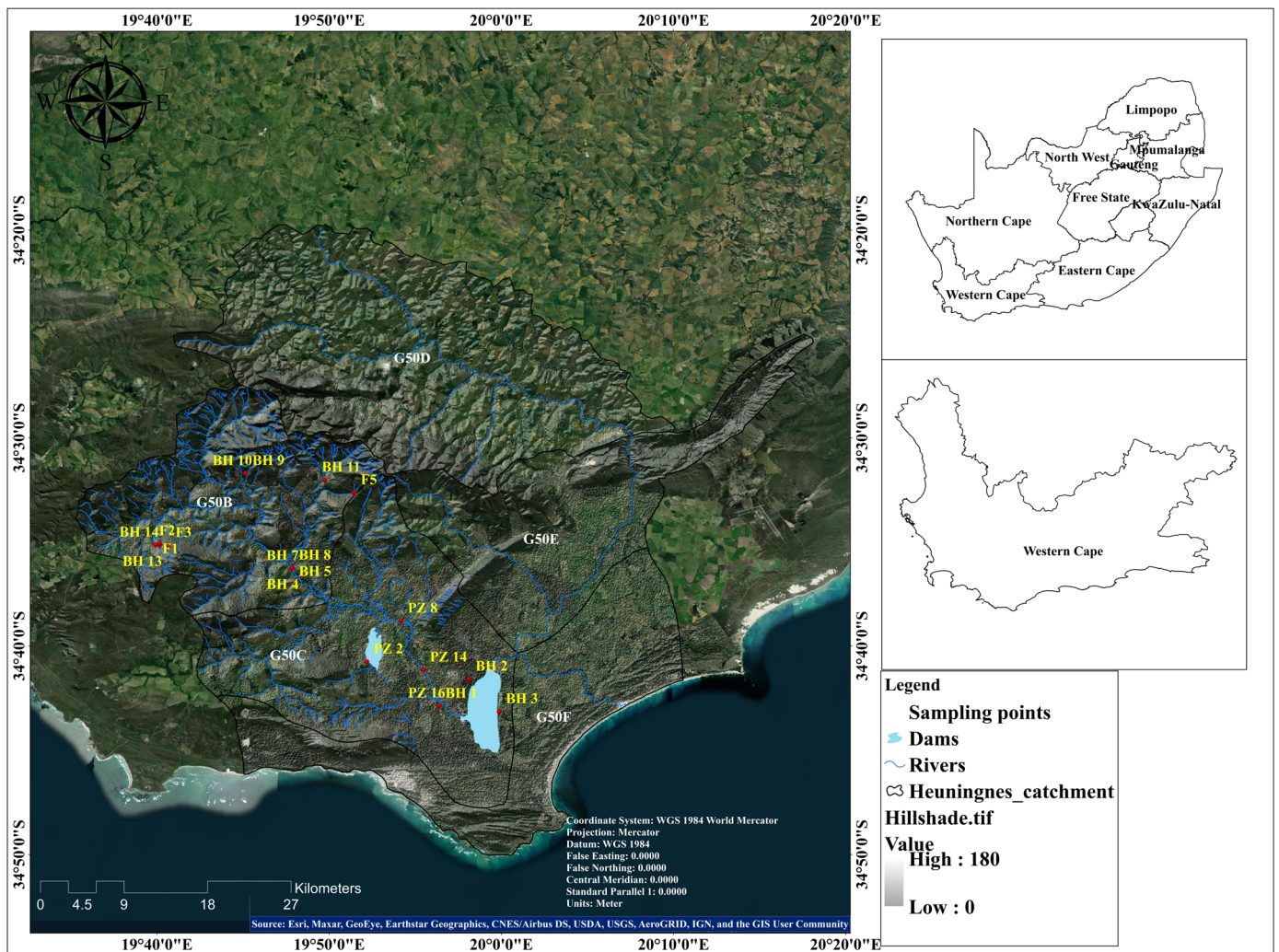
Figure 1. (**a**) The location of Heuningnes Catchment, South Africa. (**b**) Geology and lithological logs of the sampling sites.

Table 1. Lithology and hydro-stratigraphy of the main types of geology in the Heuningnes Catchment (adapted with permission from [15]).

Group/Lithology	Rock Type	Hydrostratigraphy	Yield (L/s)	Water Quality
Alluvials	Sand/silt	High yielding	>5 L/s	Brine
Bredasdorp beds	Quaternary deposits	Limited aquifer	0.1–0.5 L/s	Brackish
Bokkeveld	Shales, sandy shales	Low yielding (fractured rock system)	0–0.1 L/s	Brackish-Saline
Table Mountain Group (TMG)	sandstone quartzite, sandstone, conglomerate	High yielding aquifer (highly fractured rock system)	>5 L/s	Fresh
Cape Granite Suite	Basement granite	Aquitard/aquiclude	-	Fresh

3. Materials and Methods

3.1. Groundwater Sampling

To assess saltwater intrusion in the Heuningnes Catchment, 29 groundwater samples were taken from a coastal aquifer using piezometers and existing boreholes. Some of the piezometers were dry or broken, and some of the boreholes that were initially chosen for the study were unavailable at the time of sampling. As a result, there are gaps in the data set, which is typical for data on water quality. Most of the boreholes and piezometers that are chosen as groundwater sample locations have been established for scientific study and are under the management of the University of the Western Cape. A Solinst TLC meter was used to measure static water level prior to sampling, and a specific depth sampler was used to capture borehole samples from certain depths inside the screen. Prior to collecting a sample, three well volumes of water were removed to get rid of any standing water to obtain a sample that would be indicative of the aquifer water quality. Polypropylene 250 mL plastic bottles were used and pre-cleaned with 10% hydrochloric acid and phosphate-free

detergent from Kimix chemicals (Cape Town, South Africa). The samples were filtered using a 0.45 μm Munktell filter (Falun, Sweden) and stored in a cooler box in the field; they were then kept at 6 °C in a refrigerator until they could be analyzed in the lab. A HACH HQ40d multimeter (Loveland, CO, USA) was used to measure the EC, pH, and temperature in the field. Overall, the analytical processes, quality assurance, quality control, and precision were built on the methodology described by APHA (2017).

3.2. Groundwater Chemical Analysis

Inductively coupled plasma optical emission spectrometry was used to analyze the major cations and anions concentration. The instrument's sensitivity and detection limit vary depending on the element. The instrument's minimum detection limits are as follows: magnesium is 0.04 mg/L, calcium is 0.02 mg/L, potassium is 5.10 mg/L, and sodium is 1.80 mg/L (Thermo Fisher Scientific, Johannesburg, South Africa). Moreover, seawater intrusion in the boreholes was investigated using the seawater fraction. Chloride is regarded as a conservative ion that is unaffected by ion exchange; this proportion is frequently determined in groundwater using chloride concentration [16]. According to [4], the concentration can be calculated as follows:

$$f_{sea} = \frac{C_{Cl,sample} - C_{Cl,fresh}}{C_{Cl,sea} - C_{Cl,fresh}} \tag{1}$$

where $C_{Cl,sample}$ denotes the level of chloride in the sample, $C_{Cl,sea}$ denotes the concentration of Cl^- in Indian Ocean, and $C_{Cl,fresh}$ denotes the concentration of Cl^- in freshwater. The freshwater sample was chosen while taking into mind the lowest electrical conductivity measurement value. Because of its high solubility, Cl^- is typically not eliminated from the system [4]. The sole sources of input are the ions in the aquifer matrix or another source of salinization, such as seawater incursion [17]. Theoretical concentrations ensuing from the conservative mixing of seawater and freshwater of each ion were calculated using the seawater fraction:

$$C_{i,mix} = f_{sea} \times C_{i,sea} + (1 - f_{sea}) \times C_{i,fresh} \tag{2}$$

where $C_{i,sea}$ and $C_{i,fresh}$ denote, respectively, ion concentrations in freshwater and seawater. The difference in concentration between the conservative mixing $C_{i,mix}$ and the measured $C_{i,sample}$ for each ion served as the simplest way to express the ionic deltas (Δ) [18], and subsequent from any chemical reaction occurring with mixing was defined as follows:

$$\Delta C_i = C_{i,sample} - C_{i,mix} \tag{3}$$

Identification and measurement of hydrogeochemical processes and probable chemical reactions which occur in the aquifer depend on calculating these ionic deltas [19,20]. Hence, when $\Delta C_i > 0$, ion i introduction to groundwater happens, and when ΔC_i is negative, ion loss relative to theoretic mixing is indicated [20].

3.3. Geochemical Modeling and Rock Geochemistry

The PHREEQC geochemical modeling code is based on the collected chemical analyses, which included concentrations of both major and trace elements [21]. Using the PHREEQC, the saturation indices (SIs) for minerals of interest are calculated. The index determines the thermodynamic potential of a solution for additional mineral dissolution or precipitation. Applicable mineral saturation indices (SIs) are calculated using the formula SI = log (IAP/KT), where IAP stands for the ion activity product and KT for the solubility product. Before the model was run, the database also had the additional parameters Eh and pH. The model outputs were tabulated with a focus on the minerals that saturated the groundwater under study.

3.4. Stable Isotope Analysis

The Earth Sciences Department at the University of the Western Cape used an LGR DLT-100 Liquid Water Isotope Analyzer (Model 908-0008-2010), manufactured by Los Gatos Research Inc. (San Jose, CA, USA) to measure stable ambient isotopes of oxygen and hydrogen. Using the delta (δ) notation from the equation, the results were expressed as a deviation from the Vienna Standard Mean Ocean Water (VSMOW) in terms of per mil (‰) difference:

$$\delta^{18}O(\delta 2H) = \left(\frac{R_{sample}}{R_{standard}} - 1 \right) * 1000 \tag{4}$$

where R is the ratio of the isotopes $^{18}O{:}^{16}O$ and $^2H{:}^1H$ in the sample and the standard, respectively. The sample ratios were calibrated against the VSMOW2 and SLAP2 standard reference materials utilizing a variety of standards (high and low). For ^2H and ^{18}O, respectively, the measurement accuracy was less than 0.6 and 0.2. The local meteoric water line and the global meteoric water line (GMWL) were shown alongside the derived stable isotope data for reference. ArcGIS 10.3 Spatial Analysis Module's IDW (Inverse Distance Weighted) algorithm was used to produce a spatial distribution of the water quality characteristics.

4. Results and Discussion

4.1. Hydrogeochemical Analysis (Groundwater Facies)

The Piper trilinear plot [22] and an HFE-D diagram were utilized to clarify hydrogeochemical processes taking place in the groundwater system. The samples were classified as NaCl types originating from coastal regions (Figure 2). The NaCl-type water typically indicates that seawater had a considerable impact in coastal areas.

1. Secondary saline water (Ca^{2+} - Cl^- type)
2. Seawater (Na^+ - Cl^- type)
3. Primary alkine water (Na^+ - HCO_3^- type)
4. Freshwater (Ca^{2+} - Mg^{2+} type)
5. Mixed Ca^{2+} - Na^+ - HCO_3^- type
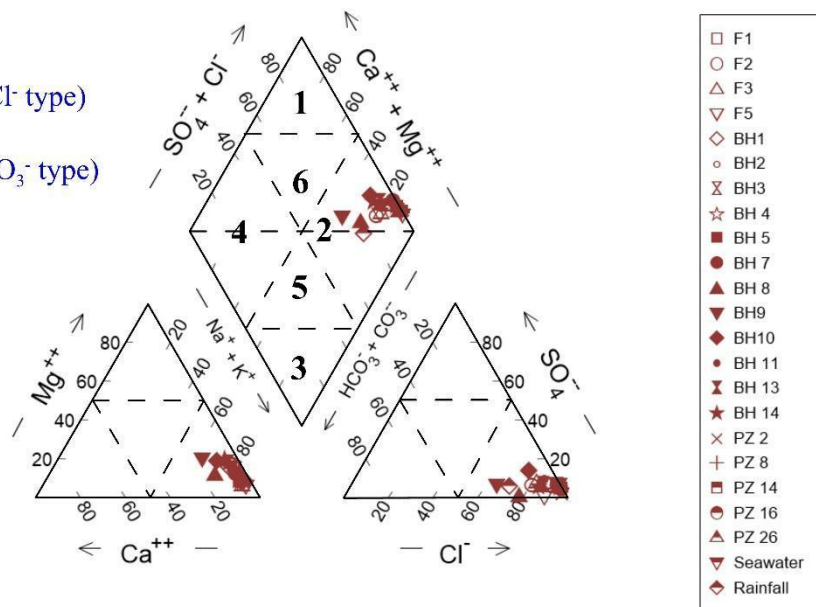6. Mixed Ca^{2+} - Mg^{2+} - Cl^- type

Figure 2. Piper trilinear diagram for groundwater samples.

The facies evolution sequence during recharge and incursion episodes may not always be clearly recognized using traditional representations such as the Piper diagram. Ref. [23] asserted that the HFE-D diagram is more useful in this context. The HFE diagram for groundwater samples from the Heuningnes Catchment is presented in Figure 3. The Na-Cl quadrant, where the samples were concentrated, demonstrates the effect of saltwater intrusion. Most of the water samples matched the facies sequence (4-7-10-13) along the mixing line, thus indicating straightforward mixing with little to no base exchange reaction

involvement. During the seawater intrusion phase, to the right and below the horizontal line of 33.3%, there was a brief reverse exchange of Na^+/Ca^{2+} and an initial increase in salinity.
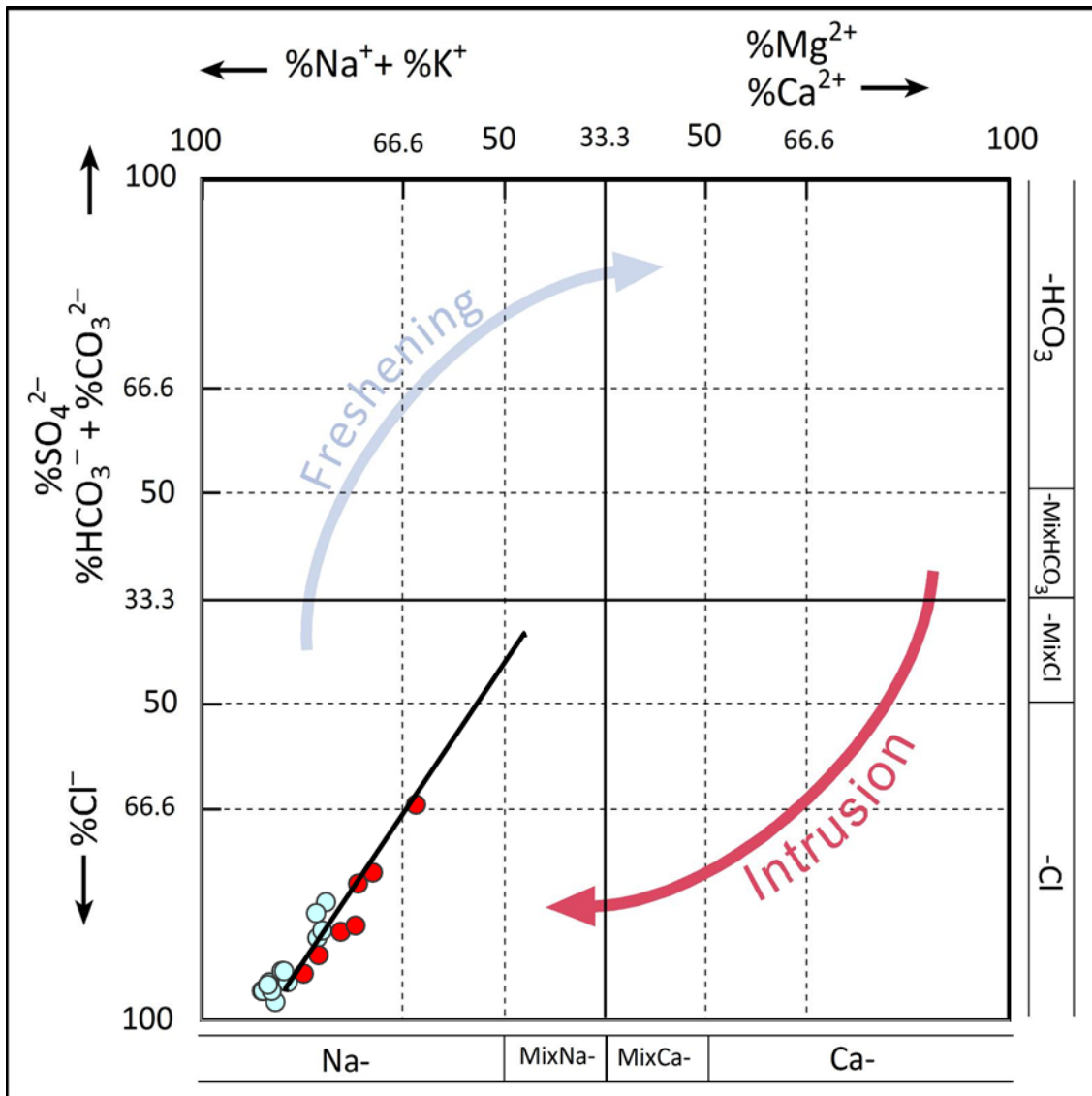

Figure 3. HFE-D diagram for groundwater samples from the Heuningnes Catchment.

4.2. Classification of Groundwater Salinization

A multiparameter water quality probe was used to take EC readings in the field. The formula TDS (mg/L) = 0.65 × EC (μS/cm) was used to indirectly determine the total dissolved solids (TDS) values of groundwater from the EC values [24]. Using the classification of [25], TDS values were utilized to demonstrate the salinization level. The brackish and brine water were considered to be saline in this study based on the salinity categorization in Table 2.

Table 2. Classification of groundwater salinization in Heuningnes Catchment.

Site Name	TDS	Salinization	
F1	380.00	Fresh water	Upstream
F2	299.00	Fresh water	Upstream
F3	218.00	Fresh water	Upstream
F5	265.00	Fresh water	Upstream
BH1	19,435.00	Saline water	Downstream
BH2	39,520.00	Saline water	Downstream
BH3	13,449.00	Saline water	Downstream
BH 4	11,096.00	Saline water	Downstream
BH 5	14,755.00	Saline water	Downstream
BH 7	8346.00	Brackish water	Downstream
BH 8	1976.00	Brackish water	Downstream
BH9	235.00	Fresh water	Upstream
BH10	259.00	Fresh water	Upstream
BH 11	463.00	Fresh water	Upstream
BH 13	291.00	Fresh water	Upstream
BH 14	303.00	Fresh water	Upstream
PZ 2	20,150.00	Saline water	Downstream
PZ 8	35,165.00	Saline water	Downstream
PZ 14	43,030.00	Saline water	Downstream
PZ 16	21,450.00	Saline water	Downstream
PZ 26	41,795.00	Saline water	Downstream

Groundwater TDS values range from 218 mg/L to 43,030 mg/L. There was a clear distinction of groundwater between upstream and downstream areas. The upper high elevation part of the catchment contained fresh water with the highest TDS values of 463 mg/L and an average of 301 mg/L (Table 2). The upstream part of the catchment was dominated by the TMG formation with sandstone and quartzite rocks of weathered and fractured units [26]. The lower TDS values may be attributed to the high flow rate of groundwater and lower solubility of the aquifer material units. The low TDS values for the TMG formation were due to the less reactive nature of its quartzite sandstone rock, as well as the high localized rainfall in the mountainous terrain where the TMG is prevalent [27]. Meanwhile, the middle and lower parts of the study area had the highest groundwater TDS values with an average of 22,514 mg/L. The elevated TDS values could be due to the mineral dissolution, as the area is dominated by the Bokkeveld shale and clay formations. The low permeability in these formations, coupled with a gentle slope, may have resulted in slow groundwater velocities, as well as high residence and contact times resulting in high rock–water interactions and, therefore, elevated salinization. In general, there was a correlation between the potentiometric surface and groundwater salinity such that the groundwater in upstream areas was fresh and the salinity increased in downstream areas.

4.3. Suitability of Groundwater for Drinking

Depending on the specific regulations, the quality of groundwater influences its usefulness for diverse applications. Only the physicochemical parameters of the research area's groundwater quality were compared with industry-standard values from the [28] drinking purpose standards in order to determine its acceptability for drinking (Figure 4). TDS values constitute an important water quality parameter, which is widely used to assess the suitability of water for drinking and irrigation purposes. High values of TDS in groundwater may affect persons who are suffering from kidney and heart diseases. The high content of TDS in water can be due to anthropogenic sources such as domestic sewage, septic tanks, and agricultural activities. Higher concentrations of TDS cause gastrointestinal irritation in humans and may also lead to laxative effects [5]. The maximum permissible limit of TDS in drinking water is 1000 mg/L [28]. TDS values of groundwater samples of the study area showed that 43% of water was under the highest desirable limit, thus indicating that they can be used for drinking purposes without any risk. The sites with

drinkable water were in the upstream section of the catchment that is dominated by the TMG formation.
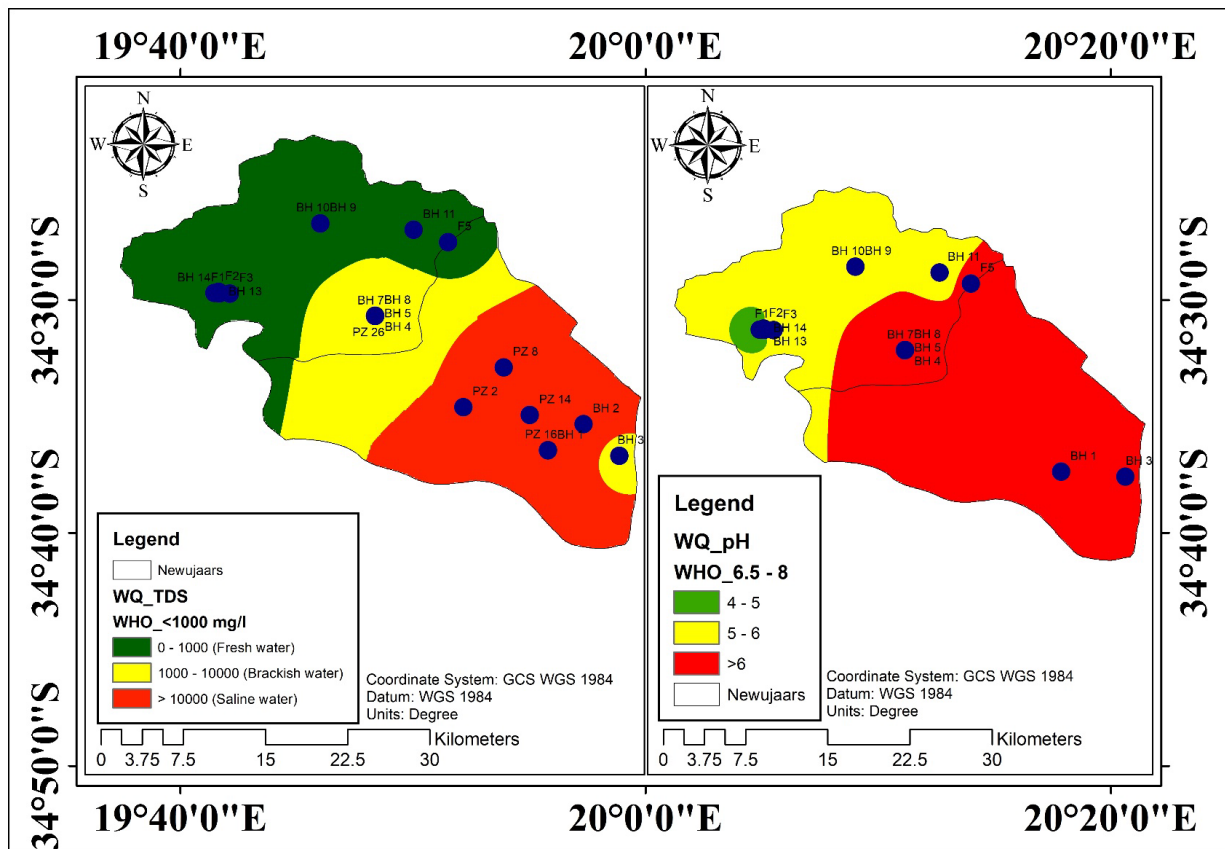

Figure 4. Groundwater physicochemical parameters distribution.

4.4. Saltwater Intrusion Analysis

4.4.1. Major Ion Indicators

Sources of salinity and the process of buildup are intimately linked to groundwater salinity. The weathering, dissolution, and recharging of aquifers by saline water bodies are potential sources of salinity in the coastal aquifer. The process of enrichment raises the salinity of groundwater through a greater dissolution capability as pressure and temperature vary. The ratios of Ca^{2+}/Cl^-, Na^+/Cl^-, and Br^-/Cl^- are displayed against (Cl and TDS) in Figure 5A–D, respectively. The Na^+/Cl^- ratio, for instance, would remain constant as salinity increased in groundwater where evaporation predominated [29]. The positive correlation between the Na^+/Cl^- ratio and the groundwater salinity within the study area pointed to the domination of evaporation or saltwater mixing as the sources of salinity. Br was mostly found in seas and had stable features; it is rarely engaged in chemical reactions, and the ratio of Br^-/Cl^- in seawater was about 0.0015 [30]. Therefore, if seawater incursion or palaeo-saltwater incursion were the main sources of recharge in the coastal aquifer, the Br^-/Cl^- ratio would not change as salinity rose. When groundwater salinity increased, the Na^+/Cl^- and Br^-/Cl^- ratios (in Figure 5E,F) remained constant, and the ratios of brackish and saline water were comparable to those of seawater and brine (palaeo-saltwater).
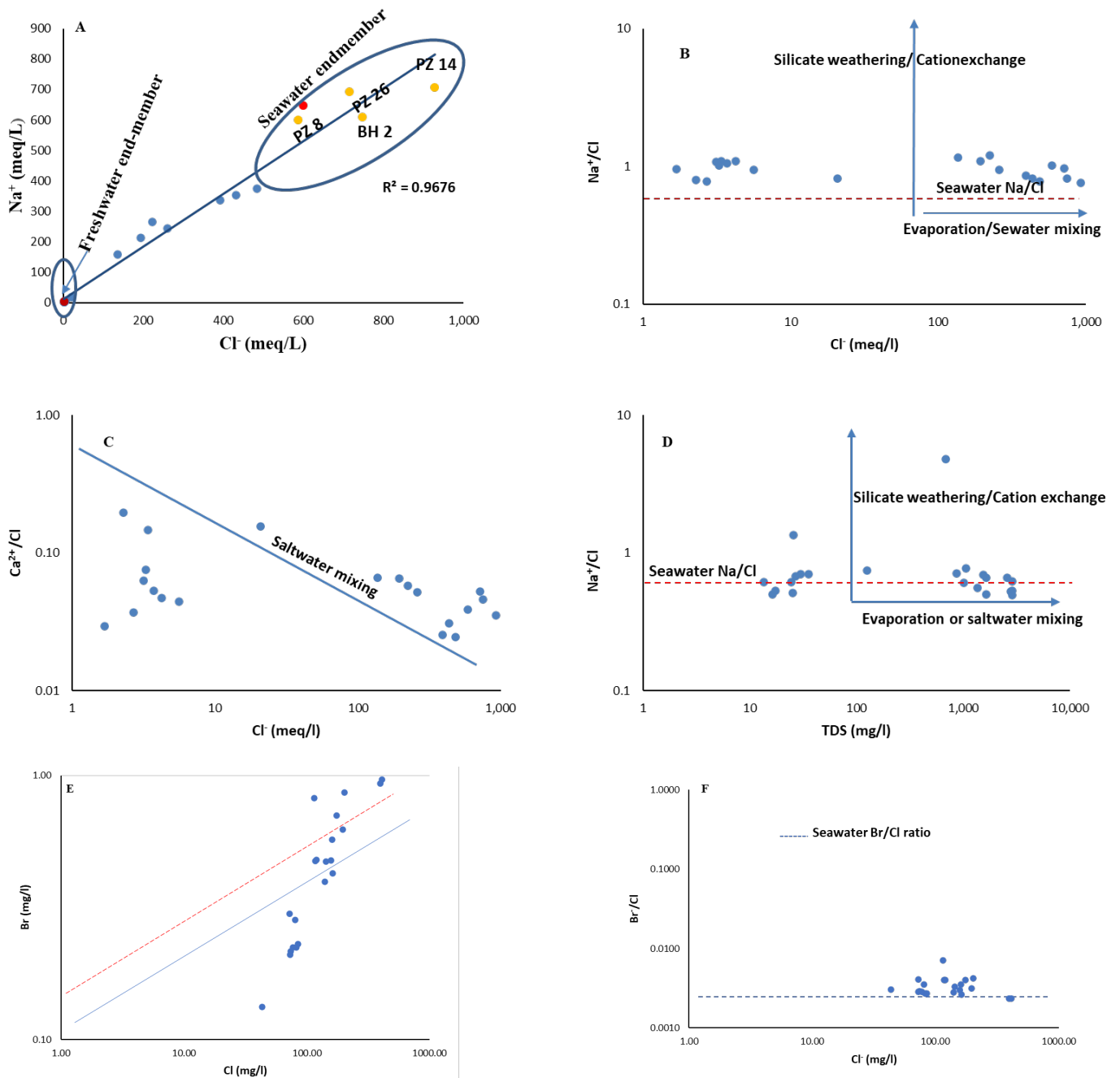
Figure 5. Bivariate plots for elucidating salinity sources for groundwater (**A–D**) and the mixing process of saltwater intrusion are reflected in the hydrochemical relationships for a few selected ions and ionic ratios (**E,F**).

The findings suggest that, after palaeo-seawater intrusion, water–rock interactions were the major cause of the salinity increase (e.g., mineral weathering and ion exchange). Data showing the Br^-/Cl^- and Na^+/Cl^- ratios of saltwater and brine were equivalent to those of the seawater and surrounding freshwater, thus suggesting that evaporation also contributed significantly to the increase in groundwater salinity [31]. In Figure 5, the theoretical mixing line and the seawater Br^-/Cl^- ratio line was parallel, and the distribution of the water samples was linear between the two lines for 45% of the samples. Furthermore, 55% of the water samples were distributed evenly along the mixing line in Figure 5, thereby demonstrating that the salinity in the groundwater was a result of the intrusion from saltwater, which included both seawater and palaeo-saltwater.

4.4.2. Seawater Intrusion Quantification

There was an extensive range of seawater inputs to groundwater inputs, in the range of 1–74%, when Equation (1) was applied to the data. Seawater fractions were significantly higher (>50%) in the lower parts of the catchment than they were in the upper parts (50%). In a similar study by [32], they found seawater fractions to be less than 1%; this could be a result of the artificial exploitation of the aquifer system. While some samples were Ca^{2+}-deficient, several of the samples exhibited excess Ca^{2+} (Table 3). This did not, however, take into consideration the Na^+ deficiency or enrichment that was caused by source- or process-related effects in most of the samples. The dissolution or precipitation of the carbonate minerals in the aquifer may have caused Ca^{2+} enrichment or depletion (Table 3). In contrast to rock-controlled geochemical processes, Ca^{2+} and Na^+ behaved similarly in the studied samples, and the quantities of Na^+ and Ca^{2+} reactions exhibited a strong positive correlation (r = 0.84). The opposing behavior of Na^+ and Ca^{2+} may be explained by cation exchange activities and the dilution dominance of seawater over freshwater in the coastal aquifer.

Table 3. Seawater fraction calculation.

Sample ID	Seawater Fraction	Ca^{2+} (Mix)	Ca (React)	Na^+ (Mix)	Na (React)	K^+ (Mix)	K (React)	Mg^{2+} (Mix)	Mg (React)	Cl^- (Mix)	Cl (React)	SO_4^{2-} (Mix)	SO_4 (React)	HCO_3^- (Mix)	HCO_3 (React)
F1	0.00	0.15	0.05	1.92	2.69	0.13	−0.08	0.41	0.49	1.95	2.30	0.15	0.20	0.62	−0.32
F2	0.00	0.00	0.20	0.01	3.90	0.00	0.05	0.00	0.82	0.01	3.72	0.00	0.29	0.00	0.59
F3	0.00	0.00	0.05	0.00	1.61	0.00	0.03	0.00	0.33	0.00	1.68	0.00	0.15	0.93	−0.73
F5	0.00	0.00	0.10	0.00	2.09	0.00	0.05	0.00	0.41	0.00	2.70	0.00	0.02	0.00	0.30
BH1	**0.65**	6.49	3.49	219.05	117.95	0.99	0.54	21.92	11.81	254.28	136.92	12.40	6.67	2.88	1.55
BH2	**1.25**	43.09	−8.51	758.42	−149.72	2.90	−0.57	52.28	−10.32	932.11	−184.01	56.01	−11.06	6.94	−1.37
BH3	0.43	5.81	7.66	105.44	139.16	0.59	0.79	10.29	13.57	112.13	147.97	6.79	8.95	3.11	4.10
BH 4	0.32	4.06	8.61	67.92	144.08	0.06	0.14	7.12	15.09	62.09	131.71	3.41	7.23	0.83	1.76
BH 5	0.37	4.72	8.10	98.12	168.18	0.10	0.18	10.61	18.18	82.02	140.58	6.39	10.95	0.83	1.43
BH 7	0.22	2.03	7.00	35.44	122.16	0.05	0.18	5.18	17.86	30.72	105.88	2.07	7.15	0.47	1.60
BH 8	0.03	0.10	3.14	0.54	16.50	0.00	0.10	0.09	2.62	0.66	20.14	0.01	0.18	0.18	5.46
BH9	0.00	0.00	0.45	0.00	1.83	0.00	0.05	0.00	0.58	0.00	2.30	0.00	0.23	0.00	0.98
BH10	0.00	0.00	0.50	0.01	3.69	0.00	0.10	0.00	0.99	0.01	3.39	0.00	0.60	0.00	0.46
BH 11	0.01	0.00	0.25	0.03	5.27	0.00	0.03	0.01	1.06	0.03	5.59	0.00	0.60	0.00	0.36
BH 13	0.00	0.00	0.20	0.01	3.38	0.00	0.05	0.00	0.82	0.01	3.14	0.00	0.27	0.00	0.26
BH 14	0.00	0.00	0.25	0.01	3.34	0.00	0.05	0.00	0.90	0.01	3.29	0.00	0.21	0.00	0.39
PZ 2	**0.72**	9.57	3.75	253.95	99.35	0.88	0.35	25.43	9.95	310.81	121.59	7.23	2.83	3.35	1.31
PZ 8	**0.98**	22.25	0.50	584.62	13.18	0.48	0.01	42.64	0.96	574.65	12.95	27.99	0.63	1.93	0.04
PZ 14	**1.55**	50.87	−17.99	1093.10	−386.60	0.94	−0.33	72.55	−25.66	1436.58	−508.08	70.89	−25.07	4.77	−1.69
PZ 16	**0.81**	9.61	2.32	302.17	72.83	0.86	0.21	29.83	7.19	390.41	94.09	16.36	3.94	3.83	0.92
PZ 26	**1.19**	44.65	−7.13	821.36	−131.16	0.15	−0.02	56.79	−9.07	850.39	−135.79	51.06	−8.15	2.89	−0.46

Note: Values in bold represent samples with a seawater fraction greater than 0.5.

Exchangeable Ca^{2+} is exchanged by Na^+ when seawater mixes with fresh groundwater, as shown in (Equation (5)):

$$Na^+ + \frac{1}{2}Ca^{2+} - X \rightarrow Na^+ - X + \frac{1}{2}Ca^{2+} \tag{5}$$
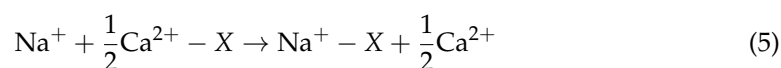
An aquifer that is saturated by seawater will have exchangers replaced by Ca^{2+} when fresh groundwater reaches it (Equation (6)):

$$Na^+ - X + \frac{1}{2}Ca^{2+} \rightarrow Na^+ + \frac{1}{2}Ca^{2+}X \tag{6}$$
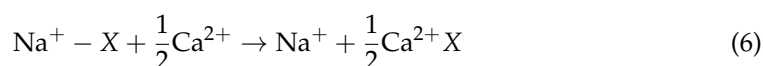
where *X* stands in for the sediment exchanger. The exchanger in the Heuningnes aquifer appeared to be the sand–clay found in the aquifer matrix, which contains iron oxides that have substantial cation exchange capacities. The presence of excess Na^+ (Na^+ React > 0) and a deficit of Ca^{2+} (Ca^{2+} React < 0) in some samples, predominantly with low salinity, suggests that saltwater influenced the ion exchange. The samples (BH2, PZ14, and PZ16) showed a lack of Na^+ (Na^+ React < 0), thereby proving that the aquifer was greatly influenced by seawater intrusion (Table 2). This was congruent with the high salinity of groundwater

of the Na-Cl type, whereas groundwater with low salinity promoted a refreshing process (Figures 2 and 3). Geochemical speciation modeling was used.

The saturation index and summary data for several mineral phases are displayed (Table 4). Calculations of the saturation index for samples of groundwater showed that halite (NaCl), calcite ($CaCO_3$), dolomite ($CaMg(CO_3)_2$), gypsum ($CaSO_4 \cdot 2H_2O$), anhydrite ($CaSO_4$), and aragonite ($CaCO_3$) phases were typically close to equilibrium to the saturation state. The concentrations of miner phases such as dolomite, gypsum, and halite were almost neutral owing to the combined influences of mineral dissolution, an incursion of seawater, and ion exchange activities. The saturation index of halite in groundwater ($-7.18 < SI < -2.06$) indicated that mineral dissolution was one of the main mechanisms for salinization. There was a moderate Ca^{2+} shortfall in some samples, which was exchanged by Na^+ and Cl^-, as indicated by the moderate correlation of Ca^{2+} and SO_4^{2-} ($R^2 = 0.68$), which suggested cation–exchange mechanisms. Gypsum precipitation and the decrease in SO_4^{2-} ions in groundwater could not be explained by the extremely low gypsum saturation index ($-4.93 < SI < 1.35$).

Table 4. Summary of saturation indices of groundwater samples.

	Calcite	Gypsum	Halite	Dolomite	Aragonite
	($CaCO_3$)	($CaSO_4 \cdot 2H_2O$)	(NaCl)	$CaMg(CO_3)_2$	($CaSO_4$)
Minimum	−5.08	−4.93	−7.18	−9.27	−5.22
Maximum	1.08	−0.50	−2.06	2.43	0.94
Mean	−1.75	−2.24	−4.55	−2.98	−1.89
Median	−0.89	−2.43	−3.63	−1.29	−1.03
Std. Dev	1.97	1.35	1.96	3.85	1.97

The fact that most samples were undersaturated with respect to calcite and dolomite could suggest the possibility of secondary carbonate precipitation (Figure 6), which was not dominant in the upper catchment but only in the lower part of the catchment. The rise in Cl^-, SO_4^{2-}, and ionic strength can be attributed to mixing with high TDS groundwater values from high salinity locations that might have had a historic seawater transgression (geological perspective) or localized evaporation pans containing saline water. Most water samples (approximately 60%) were undersaturated with respect to calcite and dolomite (SI of calcite −5.08 to 1.08; SI of dolomite −9.27 to 2.43) when it came to the dissolution and precipitation of mineral phases such as calcite, dolomite, and gypsum. According to [33], the presence of sandstone in the catchment could be the reason that most samples were undersaturated.

Calcite, dolomite, gypsum, and anhydrite versus the saturation indices (SI) are illustrated in a cross plot (Figure 7). Aragonite, dolomite, and calcite mineral phases had a poor connection with SO_4^{2-} concentrations (Figure 7A,B,D). These minerals in the carbonate phase were in a state of sub-saturation to saturation. The amount of SO_4^{2-} in the groundwater samples was low. Coastal aquifers frequently have sulphate deficiency because of seawater intrusion as cited in [34]. The SI of gypsum has a modest connection with SO_4^{2-} (Figure 7D) and was significantly undersaturated ($-4.93 < SI < -0.50$) in moderately undersaturated circumstances. However, dissolution was still occurring in the aquifer.
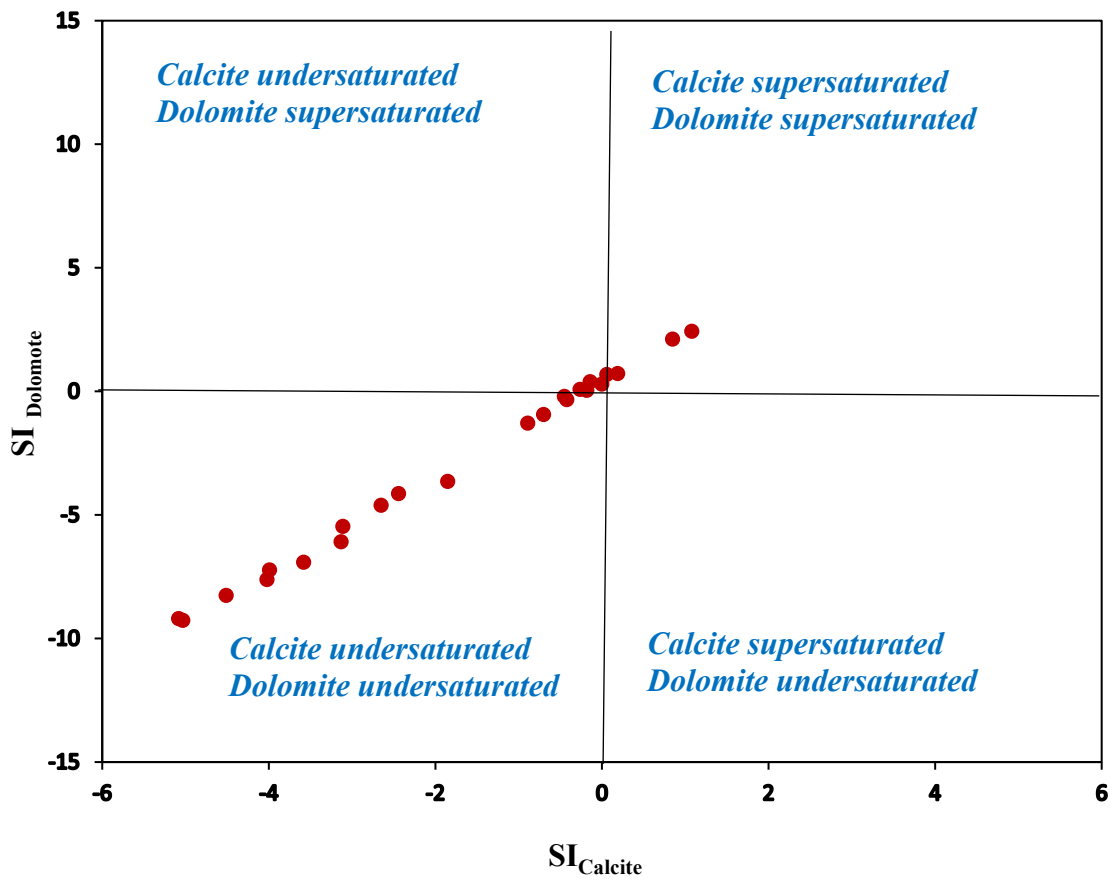
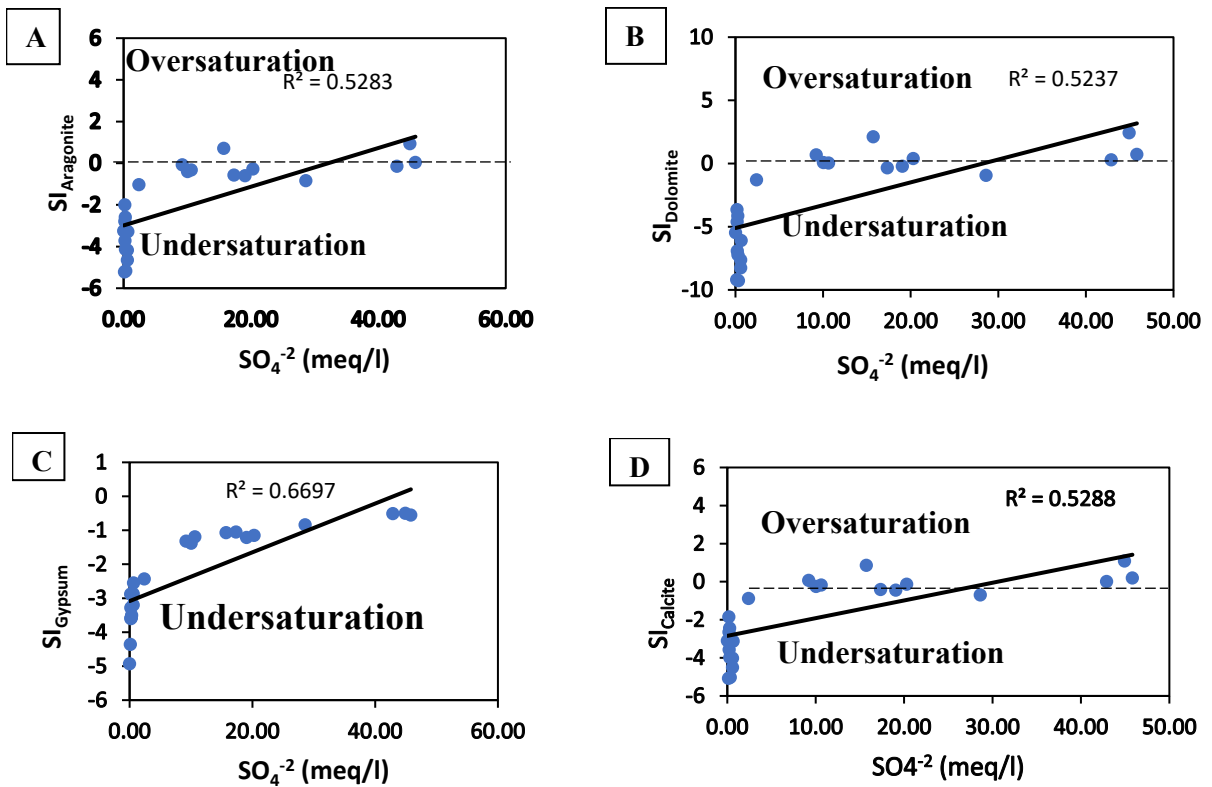**Figure 6.** Saturation indices for calcite and dolomite in Heuningnes.

Figure 7. SO_4^{2-} vs. SI of mineral phases ((**A**) aragonite; (**B**) dolomite, (**C**) gypsum, (**D**) calcite).

Minerals, including dolomite ($CaMg(HCO_3)_2$), calcite ($CaCO_3$), and gypsum($CaSO_4 \cdot 2H_2O$), were prominent soluble mineral components according to hydrogeochemical investigations of groundwater samples. Mineral indices such as dolomite, gypsum, and halite were sub-saturated to near-equilibrium, while calcite, anhydrite, and aragonite were undersaturated. Investigation of the saturation indices showed that dolomite saturation was more common than the calcite saturation. All mineral phases had saturation indices that were less than zero, thus indicating that they can dissolve in groundwater. Mineral dissolution also contributed to the salinization of the groundwater.

4.5. Identification of Groundwater Origin by $\delta^{18}O$ and δ^2H Analyses

To know the source of groundwater salinity, the stable isotopes of ^{18}O and ^2H can be enriched and depleted to disclose information about precipitation, surface water evaporation, and ocean sources. The study catchment and Cape Town are characterized by the Mediterranean climate, so the study employed the LMWL of Cape Town. The incursion of seawater in groundwater has been studied at several places throughout the world using ^{18}O and ^2H values [35,36]. In Cape Town, which is in the Western Cape [14], it was reported that the long-term weighted mean values of $\delta^{18}O$ and δ^2H rainfall ranged from 4.1‰ to 21‰, respectively. Regarding the Global Meteoric Water Line (GMWL), the relationship between δ^2H and $\delta^{18}O$ was also specified as $\delta^2H = 8\delta^{18}O + 10‰$ [34].

The examined groundwater's isotopic composition exhibited a wide range of $\delta^{18}O$ values (−5.4‰ to −0.5‰) and δ^2H values (−25.6‰ to 1.6‰) during the wet season and $\delta^{18}O$ values (−5.5‰ to −0.9‰) and δ^2H values (−25.9‰ to −3.3‰) during the dry season (Table S1). All ranges conformed with [14] results. A conventional $\delta^{18}O$ vs. δ^2H plot is shown in Figure 8, where most groundwater samples were flanked by the local and global meteoric line, thus indicating that the water has a meteoric origin and has not undergone any significant evaporation prior to recharge. This indicates that rainfall quickly recharged the aquifer via soil and the non-saturated zone as a direct recharge and that post-precipitation evaporation was not an active process during the passage through the soil. Wells with a depth of less than 20 m and one sample with a depth of 100 m had highly enriched stable isotope compositions and diverged from the LMWL and GMWL (14 out of 29 other groundwater samples) (Figure 8). These groundwater samples had relatively high $\delta^{18}O$ values (>−15.7), which plotted on a line with a slope of 6.23, which was significantly higher than the LMWL (5.28), thus suggesting that the enrichment can be due to groundwater–seawater mixing and/or the influence of evaporation [35,36].

The mixing of various water sources is the primary driver of groundwater evolution in intruded aquifers. Tracking the mixing course and quantities of different water bodies can be done by using the link between Cl and $\delta^{18}O$ as a marker [32]. The bulk of groundwater samples were distributed as freshwater members, with few samples in the brackish and saline category, as shown in Figure 9. The freshwater–seawater mixing line in the Heuningnes Catchment had equal amounts of brackish water samples, with the proportion of seawater varying from 0% to 10%. The saltwater–freshwater mixing line was surrounded by samples of saline water, with the amount of brine varying from 5% to 30%. As a result, most of the saltwater in Heuningnes Catchment followed a freshwater–brine mixing trajectory, thus implying the presence of a palaeo-saltwater incursion.
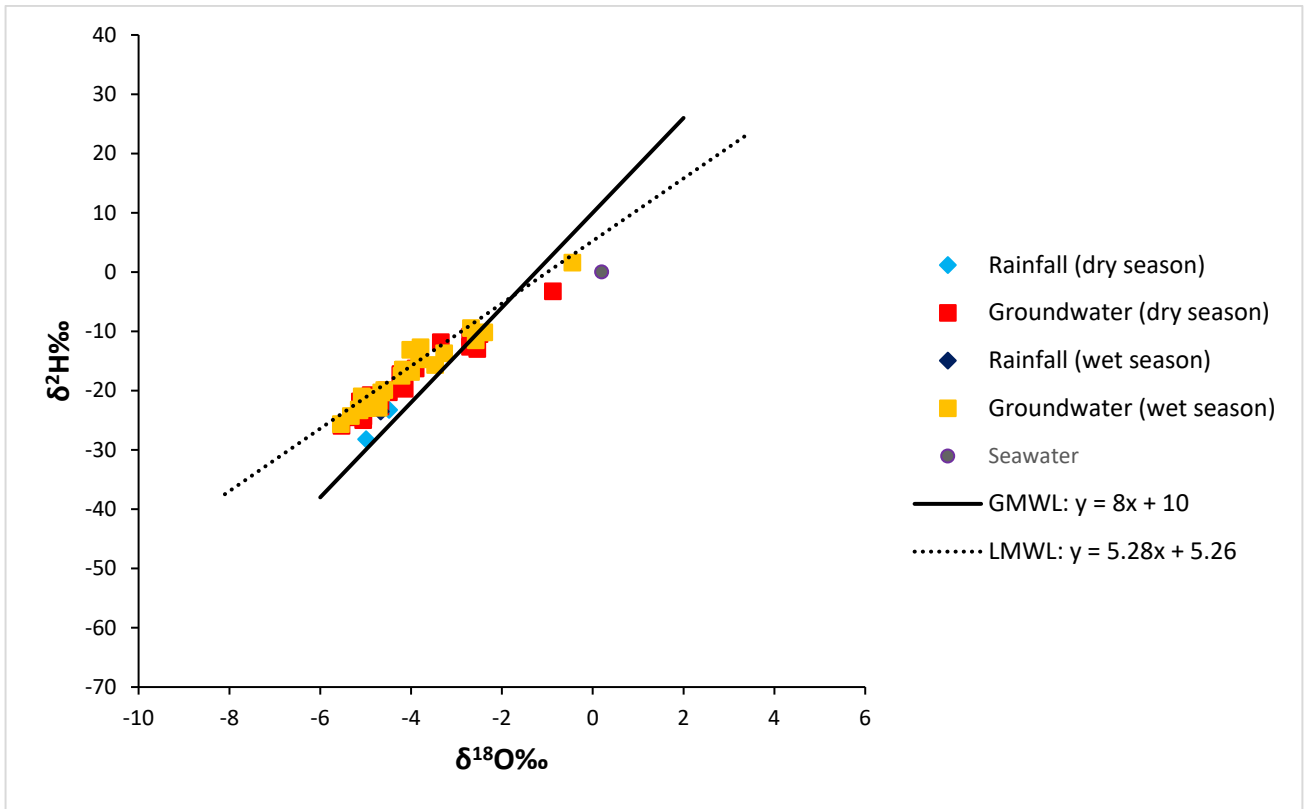
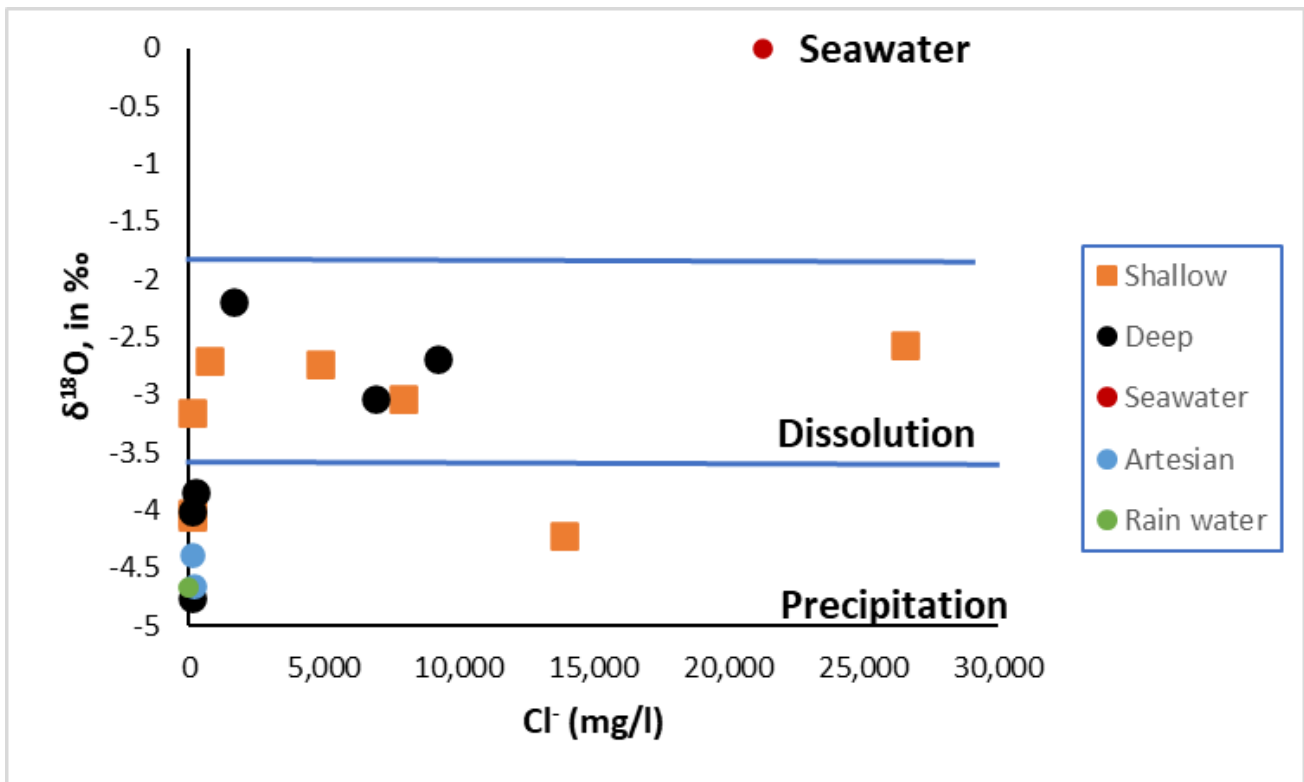**Figure 8.** Illustration of stable isotopes of oxygen (^{18}O) and hydrogen (^{2}H) compositions.

Figure 9. Illustration of Cl and δ^{18}O for tracing mixing of different waters.

5. Conclusions

This study revealed that the chemical compositions of groundwater of the coastal aquifer were influenced by hydrogeochemical processes, seawater incursion, rock–water interactions, ion exchange, and mineral saturation. The most common groundwater facies in the catchment were Na-Cl, which indicated the influence of seawater. The importance of seawater mixing for coastal aquifers was demonstrated by the fact that the molar ratio of (Na^+/Cl^-) (0.83) was close to the ideal mixing interface (0.86) between seawater and freshwater. Ionic ratios used to estimate the hydrogeochemical properties of the coastal aquifer revealed a strong conformity with the mixing lines of freshwater and saltwater endmembers, thus highlighting the significance of mixing in natural settings. Few samples had seawater concentrations above 50%, and the range of seawater in groundwater was from 0.01 to 43%. Groundwater chloride levels (81.5 to 26,557.5 mg/L) and oxygen isotope ($\delta^{18}O$) values (-5.5‰ to -0.9‰) indicated that freshwater and saltwater resources were mixing in the saline end member. The isotopic results showed that groundwater composition was significantly influenced by evaporation processes and seawater mixing. According to the groundwater hydrochemistry and isotopic compositions, brine or palaeo-saltwater intrusion was the main cause of groundwater salinity in the study area. The intermediate to lower reaches of the catchment's groundwater was influenced by the palaeo-saltwater intrusion. The correlations between the Na^+/Cl^- and Br^-/Cl^- and groundwater salinity showed that saltwater intrusion was the main cause of salinity, followed by water–rock interactions and evaporation. The fact that saltwater and brine have Na^+/Cl^- and Br^-/Cl^- ratios that are identical to those of saltwater and neighboring freshwater serves as evidence that evaporation has a role in the rise in groundwater salinity. The findings of this study are crucial to the National Water Resources Strategy (NWRS) of South Africa for establishing water quality monitoring networks. These findings will serve as baseline conditions for the system to monitor if the intrusion is moving landwards or if it is receding.

Supplementary Materials: The following supporting information can be downloaded at: https://www.mdpi.com/article/10.3390/w15112141/s1, Table S1: Isotopic composition of groundwater and rainfall samples.

Author Contributions: Conceptualization, T.K.; Data curation, A.X.; Formal analysis, A.X.; Investigation, A.X. and T.K.; Resources, S.C.; Validation, S.C.; Writing—original draft, A.X.; Writing—review and editing, H.W.T.M. and T.A.A. All authors have read and agreed to the published version of the manuscript.

Data Availability Statement: The dataset generated and/or analyzed during the current study is not publicly available due to further dissertation writing but are available from the corresponding authors upon reasonable request.

Conflicts of Interest: The authors declare no conflict of interest.

References

1. Ktépi, B. Environmental Science. In *Green Technology: An A-to-Z Guide*; Sage: Newbury Park, CA, USA, 2012. [CrossRef]
2. Putra, D.B.E.; Hadian, M.S.D.; Alam, B.Y.C.S.; Yuskar, Y.; Yaacob, W.Z.W.; Datta, B.; Harnum, W.P.D. Geochemistry of groundwater and saltwater intrusion in a coastal region of an island in Malacca Strait, Indonesia. *Environ. Eng. Res.* **2020**, *26*, 200006. [CrossRef]
3. Argamasilla, M.; Barberá, J.; Andreo, B. Factors controlling groundwater salinization and hydrogeochemical processes in coastal aquifers from southern Spain. *Sci. Total. Environ.* **2017**, *580*, 50–68. [CrossRef] [PubMed]
4. Appelo, C.A.J.; Postma, D. *Geochemistry, Groundwater and Pollution*, 2nd ed.; A.A Balkema Publishers: Amsterdam, The Netherlands, 2005; p. 649, ISBN 978-0415364287.
5. Diédhiou, M.; Ndoye, S.; Celle, H.; Faye, S.; Wohnlich, S.; Le Coustumer, P. Hydrogeochemical Appraisal of Groundwater Quality and Its Suitability for Drinking and Irrigation Purposes in the West Central Senegal. *Water* **2023**, *15*, 1772. [CrossRef]
6. Fan, X.; Min, T.; Dai, X. The Spatio-Temporal Dynamic Patterns of Shallow Groundwater Level and Salinity: The Yellow River Delta, China. *Water* **2023**, *15*, 1426. [CrossRef]

7. Kumar, P.; Kumar, A.; Singh, C.K.; Saraswat, C.; Avtar, R.; Ramanathan, A.L.; Herath, S. Hydrogeochemical Evolution and Appraisal of Groundwater Quality in Panna District, Central India. *Expo. Health* **2016**, *8*, 19–30. [CrossRef]

8. Ghezelsofloo, E.; Raghimi, M.; Mahmoodlu, M.G.; Rahimi-Chakdel, A.; Khademi, S.M.S. Saltwater intrusion in drinking water wells of Kordkuy, Iran: An integrated quantitative and graphical study. *Environ. Earth Sci.* **2021**, *80*, 520. [CrossRef]

9. Han, D.; Kohfahl, C.; Song, X.; Xiao, G.; Yang, J. Geochemical and isotopic evidence for palaeo-seawater intrusion into the south coast aquifer of Laizhou Bay, China. *Appl. Geochem.* **2011**, *26*, 863–883. [CrossRef]

10. Hoekstra, T.; Waller, L. (Eds.) *De Mond Nature Reserve Complex: Protected Area Management Plan*; CapeNature: Cape Town, South Africa, 2014; *unpublished report*.

11. Kinoti, I.K. Integrated Hydrological Modeling of Surface and Groundwater Interactions in Heuningnes Catchment (South Africa). 2018. Available online: https://webapps.itc.utwente.nl/librarywww/papers_2018/msc/wrem/kinoti.pdf (accessed on 15 December 2022).

12. Price, M. *Introducing Groundwater*; Routledge: London, UK, 1996; 296p, ISBN 9780748743711.

13. Lasher, C. Application of Fluid Electrical Conductivity Logging for Fractured Rock Aquifer Characterisation at the University of the Western Cape's Franschhoek and Rawsonville Research Sites. Ph.D. Thesis, University of the Western Cape, Cape Town, South Africa, 2011.

14. Banda, S.D.V. Assessing Hydrogeological Characteristics to Establish Influence of Aquifer-River Interaction in Non-Perennial River Systems, Heuningnes Catchment. Master's Thesis, University of the Western Cape, Cape Town, South Africa, 2019.

15. Manyama, K. Hydrogeophysical Characterization of Shallow Coastal Aquifers in the Western Cape, South Africa. Master's Thesis, University of the Western Cape, Cape Town, South Africa, November 2017.

16. Custodio, E.; Bruggeman, G.A. Groundwater problems in coastal areas. In *Studies and Reports in Hydrology*; No. 45, International Hydrological Programme (IHP); UNESCO: Paris, France, 1987.

17. Kouzana, L.; Ben Mammou, A.; Felfoul, M.S. Seawater intrusion and associated processes: Case of the Korba aquifer (Cap-Bon, Tunisia). Surface geosciences (hydrology-hydrogeology). *Comptes Rendus Geosci.* **2009**, *341*, 21–35. [CrossRef]

18. Fidelibus, M.D. Environmental Tracing in Coastal Aquifers: Old Problems and New Solutions. In *Coastal Aquifers Intrusion Technology: Mediterranean Countries*; IGME: Madrid, Spain, 2003; Volume II, pp. 79–111.

19. Pulido-Leboeuf, P. Seawater intrusion and associated processes in a small coastal complex aquifer (Castell de Ferro, Spain). *Appl. Geochem.* **2004**, *19*, 1517–1527. [CrossRef]

20. Grassi, S.; Cortecci, G. Hydrogeology and geochemistry of the multilayered confined aquifer of the Pisa plain (Tuscany—Central Italy). *Appl. Geochem.* **2005**, *20*, 41–54. [CrossRef]

21. Parkhurst, B.D.L.; Appelo, C.A.J. *User's Guide to PHREEQC (VERSION 2)—A Computer Program for Speciation, and Inverse Geochemical Calculations*; U.S. Geological Survey Water-Resources Investigations Report; U.S. Department of the Interior: Washington, DC, USA, 1999.

22. Piper, A.M. A graphic procedure in the geochemical interpretation of water-analyses. *Eos Trans. Am. Geophys. Union* **1944**, *25*, 914–928. [CrossRef]

23. Giménez-Forcada, E. Use of the Hydrochemical Facies Diagram (HFE-D) for the evaluation of salinization by seawater intrusion in the coastal Oropesa Plain: Comparative analysis with the coastal Vinaroz Plain, Spain. *HydroResearch* **2019**, *2*, 76–84. [CrossRef]

24. Lin, L.; Lin, H.; Xu, Y. Characterisation of fracture network and groundwater preferential flow path in the Table Mountain Group (TMG) sandstones, South Africa. *Water SA* **2014**, *40*, 263–272. [CrossRef]

25. Freeze, A.R.; Cherry, J.A. *Groundwater*, 1st ed.; Prentice Hall: Englewood Cliffs, NJ, USA, 1979.

26. Cumings, J.N. Biochemical aspects. *Proc. R. Soc. Med.* **1962**, *55*, 1023–1024. [PubMed]

27. Jankowski, J.; Acworth, R.I. Impact of debris-flow deposits on hydrogeochemical processes and the development of dryland salinity in the Yass River catchment, New South Wales, Australia. *Hydrogeology* **1997**, *5*, 71–88. [CrossRef]

28. Xiong, G.; An, Q.; Fu, T.; Chen, G.; Xu, X. Evolution analysis and environmental management of intruded aquifers of the Dagu River Basin of China. *Sci. Total. Environ.* **2020**, *719*, 137260. [CrossRef]

29. Guangnan, A.; Hao, K.; Rongbing, F.; Damao, X.; Jia, L. Investigation on the Hydrogeochemical Characteristics and Controlling Mechanisms of Groundwater in the Coastal Aquifer. *Water* **2023**, *15*, 1710.

30. Thabrez, M.; Parimalarenganayaki, S. Assessment of Hydrogeochemical Characteristics and Seawater Intrusion in Coastal Parts of Mangaluru City, Karnataka, India. *Water Air Soil Pollut.* **2023**, *234*, 251. [CrossRef]

31. Xaza, A. Investigating Hydrogeochemical Processes of Groundwater, Heuningnes Catchment, South Africa. Master's Thesis, University of the Western Cape, Cape Town, South Africa, 2020, *unpublished*.

32. Han, D.M.; Song, X.F.; Currell, M.J.; Yang, J.L.; Xiao, G.Q. Chemical and isotopic constraints on evolution of groundwater salinization in the coastal plain aquifer of Laizhou Bay, China. *J. Hydrol.* **2014**, *508*, 12–27. [CrossRef]

33. El Mountassir, O.; Bahir, M. The Assessment of the Groundwater Quality in the Coastal Aquifers of the Essaouira Basin, Southwestern Morocco, Using Hydrogeochemistry and Isotopic Signatures. *Water* **2023**, *15*, 1769. [CrossRef]

34. Craig, H. Isotopic variations in meteoric waters. *Science* **1961**, *133*, 1702–1703. [CrossRef] [PubMed]

35.   Vengosh, A.; Spivack, A.J.; Artzi, Y.; Ayalon, A. Geochemical and boron, strontium, and oxygen isotopic constraints on the origin of the salinity in groundwater from the Mediterranean coast of Israel. *Water Resour. Res.* **1999**, *35*, 1877–1894. [CrossRef]

36.   Kim, Y.; Lee, K.-S.; Koh, D.-C.; Lee, D.-H.; Lee, S.-G.; Park, W.-B.; Koh, G.-W.; Woo, N.-C. Hydrogeochemical and isotopic evidence of groundwater salinization in a coastal aquifer: A case study in Jeju volcanic island, Korea. *J. Hydrol.* **2003**, *270*, 282–294. [CrossRef]